Post-Print

Comparison of Filtering Techniques For Relative Attitude Estimation of Uncooperative Space Objects

Vincenzo Pesce*, Muhammad Farooq Haydar†, Michèle Lavagna‡, Marco Lovera§

Politecnico di Milano, via La Masa 34, Milano, Italy

Nowadays, one of the most active research fields in space engineering is autonomous relative navigation around uncooperative objects. A common approach used to tackle this problem is through vision-based pose determination techniques. This paper investigates the possibility of using non-linear filtering techniques to improve the attitude estimation performance of vision-based methods. Furthermore, a simulation study is presented to compare the proposed nonlinear techniques with the multiplicative extended Kalman filter for attitude estimation. First-order and second-order nonlinear filters are adapted, implemented and tested for relative attitude estimation. Finally, the consequences of uncertainty in the knowledge of the target inertia matrix are investigated.

I. Introduction

Missions involving close approaches with uncooperative space objects are becoming increasingly frequent. This kind of missions includes active debris removal, on-orbit monitoring, sample capture and close-proximity approach with small bodies. For this reason, robust, reliable and accurate algorithms for relative state estimation are necessary.

Absolute attitude estimation has been extensively studied in the past decades and several algorithms have been proposed [1, 2]. These techniques usually rely on accurate measurements of angular rate and line of sight vector. However, the accessibility of these measurements is not guaranteed when trying to estimate the relative state of an uncooperative object, especially in space. The main difference between absolute and relative attitude estimation is that, when dealing with uncooperative objects, measurements of the target angular velocity are usually not available. In fact, classical sensors exploited for relative proximity operations, such as lidar or cameras, do not provide reliable information of the angular velocity of the target body. Moreover, the measurements update frequency is usually lower due to the image-processing computational time. This lack of information inevitably affects the accuracy of the estimates and, therefore, some alternative filtering formulations have to be adopted. Several vision-based algorithms for relative pose estimation have been developed in the last few years. In particular, SLAM [3, 4] or model-based techniques [5, 6] have

---

*PhD Candidate, Department of Aerospace Science and Technology, `vincenzo.pesce@polimi.it`

†PhD Candidate, Department of Aerospace Science and Technology, `muhammadfarooq.haydar@polimi.it`

‡Associate Professor, Department of Aerospace Science and Technology, `michelle.lavagna@polimi.it`

§Full Professor, Department of Aerospace Science and Technology, `marco.lovera@polimi.it`

been extensively studied. Vision-based algorithms for relative state estimation follow two main approaches: directly processing the measurement of the feature points of an image with Kalman filters [3, 4] or using advanced image processing techniques for pose determination [7, 8]. The robustness of these approaches decreases in scenarios with high variability of pose and illumination conditions. Moreover, their performance is very sensitive to measurement noise. Model-matching techniques assume an a-priori knowledge of a 3D model of the target objects. With this information it is possible to estimate the target pose by optimizing the matches between the features (*e.g.*, corner or edges) extracted from the acquired images and the features present on the target model. As already tested in [7, 9, 10] these pose determination techniques are able to provide measurements of the relative rotation matrix. However, the results of the estimation are usually not very accurate, leading to significant errors in the attitude estimation of the target body. This makes a filtering technique downstream of the pose determination procedure indispensable.

In this work, pose measurements are assumed to be available from a monocamera system as output of a model-matching algorithm. In particular, the rotation matrix from the target to the chaser spacecraft reference frame is available. Model-matching techniques usually provide measurements of both position and orientation. In this paper, it has been assumed to decouple translational and rotational motion. For the sake of generality, this work does not provide a description of the vision-based techniques. In fact, the presented filters can be applied for relative attitude estimation in problems involving sensors that provide attitude measurements. This paper offers a comparison of different filtering techniques for relative state estimation. Starting from the case in which reliable measurements of the angular velocity are available, several cases are analyzed and discussed. The intended contributions and advancements of this paper are:

- Formulation of the relative attitude estimation problem and adaptation of nonlinear filtering algorithms for this specific application.
- A performance comparison of classical and recent nonlinear filtering techniques for relative attitude estimation.
- Investigation of the influence of the poor knowledge of the inertia matrix in filters exploiting dynamical models.

The paper is organized as follows. Section II and III present the models for filtering and a description of the filtering algorithms, respectively. In Section IV the simulation scenario is illustrated along with all the different cases analyzed in this study. Moreover, qualitative and quantitative results are presented. In Section V the conclusions are drawn.

II. Models for Filtering

In this section we describe the models for attitude dynamics and kinematics.

Attitude Kinematics   We recall that the attitude of a rigid body evolves on the Special Orthogonal group $SO(3)$, the set of 3×3 orthonormal matrices having unit determinant. The Lie algebra of $SO(3)$ is the set of 3×3 skew-symmetric matrices and is denoted by $\mathfrak{so}(3)$. For first order filtering algorithms, only the relative kinematics is necessary. The

relative attitude kinematics between two rigid bodies is given by

$$\dot{R}(t) = R(\omega(t)_\times), \quad R(0) = R_0, \tag{1}$$

where $R(t) \in SO(3)$ is the relative rotation matrix expressed in the chaser frame, and ω is the relative angular velocity expressed in the chaser frame.

The attitude kinematics can be also modeled using the quaternion representation of the attitude. We recall that the unit quaternion is a four dimensional vector, which can be defined in terms of Euler axis e and rotation angle θ as follows,

$$q = \begin{bmatrix} \varrho \\ q_4 \end{bmatrix}, \tag{2}$$

where

$$\varrho = \begin{bmatrix} q_1 & q_2 & q_3 \end{bmatrix}^T = e \sin(\theta/2), \tag{3}$$

and

$$q_4 = \cos(\theta/2). \tag{4}$$

It is apparent from the definition of the quaternion in terms of Euler axis and rotation angle, that quaternion obeys the unit-norm constraint:

$$q^T q = 1, \tag{5}$$

so that geometrically the set of all admissible quaternions spans the unit sphere in the four-dimensional Euclidean space $\mathbb{R}^4$. In this paper, we will use q to represent the relative attitude of the target object with respect to chaser spacecraft, expressed in chaser frame.

The kinematics of the (relative) quaternion is given by

$$\dot{q} = \frac{1}{2}\Omega(\omega)q = \frac{1}{2}\Xi(q)\omega, \tag{6}$$

where

$$\Omega(\omega) = \begin{bmatrix} -\omega_\times & \omega \\ -\omega^T & 0 \end{bmatrix} = \begin{bmatrix} 0 & \omega_3 & -\omega_2 & \omega_1 \\ -\omega_3 & 0 & \omega_1 & \omega_2 \\ \omega_2 & -\omega_1 & 0 & \omega_3 \\ -\omega_1 & -\omega_2 & -\omega_3 & 0 \end{bmatrix}, \tag{7}$$

and

$$\Xi(\boldsymbol{q}) = \begin{bmatrix} q_4 I_3 + \boldsymbol{\varrho}_\times \\ -\boldsymbol{\varrho}^T \end{bmatrix}, \tag{8}$$

while $\boldsymbol{\omega}$ is again the relative angular velocity expressed in the chaser frame.

Attitude Dynamics For second order filters, the equations describing the attitude for a rigid body have to be introduced. Following [4, 11], the relative attitude dynamics of the system is described as:

$$I_c \dot{\boldsymbol{\omega}} = I_c R I_t^{-1} \left[N_t - \boldsymbol{\omega}_t|_{\mathcal{T}} \times I_t \boldsymbol{\omega}_t|_{\mathcal{T}} - I_c \boldsymbol{\omega}_c \times \boldsymbol{\omega}_c - [N_c - \boldsymbol{\omega}_c \times I_c \boldsymbol{\omega}_c] \right], \tag{9}$$

where $\boldsymbol{\omega}$ and $\boldsymbol{\omega}_c$ are, respectively, the relative and chaser angular velocity expressed in the chase frame and $\boldsymbol{\omega}_t|_{\mathcal{T}}$ is the target angular velocity expressed in the target frame. I_c and I_t are the inertia matrices of chaser and target spacecraft and N_c and N_t are external torques on the chaser and target body respectively.

III. Filtering Algorithms

The problem of filtering concerns itself with finding an estimate of the state of a dynamic system based on a system model and noisy measurements. The Kalman filter is a state estimator and optimizes the MSE between the estimates and the true state, for linear systems. One of the earliest applications of the Kalman filter has been in navigation and control of aerospace vehicles, a fundamentally nonlinear problem, and that has led to many *ad hoc* extensions to the nonlinear case. The Multiplicative Extended Kalman Filter (MEKF), which is based on the local linearization of the estimation problem around the current state estimate, has been the main workhorse of real-time spacecraft attitude estimation [12]. An estimate of the mean and covariance of the state, based on second or higher-order approximations of the nonlinear functions, is used for uncertainty propagation in unscented filters [13].

Minimum energy filtering was introduced by Mortensen [14], and has been specialized to attitude estimation on the Special Orthogonal Group $SO(3)$ by Zamani et al. [15]. The nonlinear minimum energy filtering problem is infinite-dimensional, but an analytical bound on the distance to optimality has been derived for the case of second-order approximations of the minimum energy filter [16]. This second-order minimum energy filter on $SO(3)$, thanks to a geometric curvature correction term and the Lie group structure of $SO(3)$, appears to outperform the MEKF [17].

In the following we review the conventional and novel methods for attitude estimation proposed in the literature, and tailor these formulations to the problem of uncooperative attitude estimation. As highlighted in Section I, this particular problem is characterized by unavailability of angular velocity measurements. In addition, the use of image-based pose estimation techniques is computationally expensive and this mandates low update rates for the onboard applications in

space.

A. Multiplicative Extended Kalman Filter (MEKF)

The common form of the MEKF, utilizing the unit quaternion parametrization for the global attitude, is outlined in this subsection. It is worth noting that to circumvent the singularity problems of the 4×4 covariance matrix required for measurement update of a unit quaternion, the MEKF commonly relies on a *linear* measurement update based on Euler angles hence limiting the covariance matrix to 3×3.

The measured relative angular velocity $\tilde{\omega}$ approximates the true relative angular velocity ω in (6) up to a process disturbance Bw as

$$\omega = \tilde{\omega} + Bw, \tag{10}$$

where w is a zero-mean Gaussian noise process with covariance given by

$$E\left(w(t)w(\tau)^T\right) = Q(t)\delta(t - \tau).$$

For the case of uncooperative attitude estimation, please note that ω and q represent the relative angular velocity and the relative quaternion expressed in the chaser frame. It is important to underline that, since the propagation (10) is based only on the attitude kinematics, this formulation holds if expressed in any generic reference frame.

For the case of uncooperative attitude estimation, $\tilde{\omega}$ is unavailable and therefore ω is assumed to be a random process defined solely by Bw. Hence (10) becomes

$$\omega = Bw. \tag{11}$$

This seems to be a reasonable assumption if no prior information about the angular velocities of the target object and chaser spacecraft is available.

The vector measurements, typically output of a star camera, approximate the line of sight up to a noise process Dv. The measurement equation is thus given by

$$y = h(q) + Dv; \qquad h(q) = \begin{bmatrix} A(q)r_1 \\ A(q)r_2 \end{bmatrix} \tag{12}$$

where $h(q)$ is the concatenated vector of the noise-free vector measurements, A is the relative Direction Cosine Matrix (DCM), r_1 and r_2 are two mutually perpendicular directions and v is a vector of zero-mean Gaussian noise processes

with covariance given by

$$E\left(\boldsymbol{v}(t)\boldsymbol{v}(\tau)^T\right) = R(t)\delta(t - \tau).$$

In the framework of Kalman filtering, the process and measurement disturbances, $B\boldsymbol{w}$ and $D\boldsymbol{v}$, are usually taken to be Gaussian noise processes which are completely defined by a mean value and the variance.

The Kalman filtering problem can be cast into minimization of the cost function,

$$J = \frac{1}{2}E\left[\left\|\Xi^T(\boldsymbol{q}(t))\hat{\boldsymbol{q}}(t)\right\|^2\right], \tag{13}$$

where the term $\Xi^T(\boldsymbol{q}(t))\hat{\boldsymbol{q}}(t)$ represents the error between estimated and true quaternions. To solve the optimal filtering problem, the cost J is to be optimized subject to the dynamic constraints (6) and (12).

The optimization problem admits an analytical solution for the special case of linear systems. Therefore, assuming the linear propagation for the covariance matrix, one can obtain the filtering equation together with the matrix differential equation (Riccati equation) for the covariance propagation, as well as the expression for the filter gain. The complete MEKF formulation for the kinematic system defined by (6) and the line of sight measurements (12), is given in Table 1, see, e.g., [2, 18].

The $H_k(\hat{\boldsymbol{q}}_k^-)$ term in Table 1 is the linearization of $\boldsymbol{h}(\boldsymbol{q})$ based on the estimated attitude and the reference directions (of the target object measured in chaser frame). Therefore, $H_k(\hat{\boldsymbol{q}}_k^-)$ is calculated as

$$H_k(\hat{\boldsymbol{q}}_k^-) = \begin{bmatrix} \left[A(\hat{\boldsymbol{q}}_k^-)\boldsymbol{r}_1\right]_\times \\ \left[A(\hat{\boldsymbol{q}}_k^-)\boldsymbol{r}_2\right]_\times \end{bmatrix},$$

where the estimated relative attitude, *i.e.*, the relative Direction Cosine Matrix (DCM), is constructed based on the estimated quaternions as

$$A(\boldsymbol{q}) = \|\boldsymbol{q}\|^{-2}\left((q_4^2 - \|\boldsymbol{\varrho}\|^2)I_3 + 2\boldsymbol{\varrho}\boldsymbol{\varrho}^T - 2q_4\boldsymbol{\varrho}_\times\right).$$

The attitude measurement typically provided by the vision based solutions is a rotation matrix, and it can be right-multiplied by two mutually perpendicular reference directions (namely, $\boldsymbol{r}_1$ and $\boldsymbol{r}_2$) to provide two line of sight (vector) measurements, consistent with (12). These vector measurements can then be fused with the relative attitude estimates using the optimal gain, as outlined in Table 1.

It is to be pointed out that the assumption made in (11) results in trivialization of the attitude prediction step, *i.e.*, attitude prediction is switched off and only the correction step is responsible for tracking the noisy output, see Table 1.

Table 1   Multiplicative Extended Kalman Filter (MEKF)

Initialization:
$$\hat{\boldsymbol{q}}(t_0) = \hat{\boldsymbol{q}}_0, \ P(t_0) = P_0,$$

Prediction:
$$\dot{\hat{\boldsymbol{q}}} = \begin{cases} \frac{1}{2}\Xi(\hat{\boldsymbol{q}})\hat{\omega} & \text{with } \omega \text{ measurement,} \\ \boldsymbol{0} & \text{without } \omega \text{ measurement,} \end{cases}$$

$$\dot{P}(t) = F(t)P(t) + P(t)F^T(t) + BQB^T$$

$$F(t) = \begin{cases} -\hat{\omega}(t)_\times & \text{with } \omega \text{ measurement} \\ \boldsymbol{0} & \text{without } \omega \text{ measurement} \end{cases}$$

$$B = I_{3\times3}, \ Q = \sigma_w^2 I_{3\times3}$$

Correction:
$$K_k = P_k^- H_k^T \left[H_k P_k^- H_k^T + R \right]^{-1}$$

$$R = \sigma_v^2 I_{3\times3}$$

$$P_k^+ = [I - K_k H_k(\hat{\boldsymbol{q}}_k^-)]P_k^-$$

$$P_k(+) = [I - K_k H_k] P_k(-) [I - K_k H_k]^T + K_k R K_k^T$$

$$\boldsymbol{h}(\hat{\boldsymbol{q}}_k^-) = \begin{bmatrix} A(\hat{\boldsymbol{q}}_k^-)\boldsymbol{r}_1 \\ A(\hat{\boldsymbol{q}}_k^-)\boldsymbol{r}_2 \end{bmatrix}$$

$$\hat{\boldsymbol{q}}_k^+ = \hat{\boldsymbol{q}}_k^- + \frac{1}{2}\Xi(\hat{\boldsymbol{q}}_k^-)K_k \left[\boldsymbol{y}_k - \boldsymbol{h}(\hat{\boldsymbol{q}}_k^-) \right]$$

B. Minimum Energy Filter on $SO(3)$

The formulation of the minimum energy filter on $SO(3)$ is based on the perturbed kinematic model:

$$\dot{R}(t) = R(\tilde{\omega}(t)_\times + g\delta(t)), \quad R(0) = R_0, \tag{14}$$

where $R(t) \in SO(3)$ is the relative rotation matrix expressed in the chaser frame, and $g\delta(t) \in \mathfrak{so}(3)$ is the process disturbance. Since the measured relative angular velocity $\tilde{\omega}$ is not available in an uncooperative attitude estimation setup, $\dot{R}(t)$ will be assumed to be driven only by $g\delta(t)$.

The measurement $Y(t) \in SO(3)$, which is again a relative rotation matrix expressed in the chaser frame, is typically obtained through a vision-based solution. The measurement $Y(t)$ can be modeled as

$$Y(t) = R(t)\epsilon(t), \tag{15}$$

where $\epsilon(t) \in SO(3)$ is the measurement error.

The minimum-energy filtering approach aims at obtaining a state estimate $\hat{R}$ by minimizing a cost function J at each time step t, given the actual measurements (15). To obtain the state estimate $\hat{R}$, one seeks a combination of the unknowns (*i.e.,* the initial state R_0 and the process and measurement disturbances δ_0, ϵ_0) that is compatible with the actual measurements (15) and system model (1). The resulting cost function is:

$$J = \frac{1}{4}trace\left[(R_0 - I)^T K_0^{-1}(R_0 - I)\right] + \int_0^T \left(\frac{1}{2}trace\left[\delta^T(\tau)\delta(\tau)\right] + \frac{1}{4}trace\left[(\epsilon(\tau) - I)^T(\epsilon(\tau) - I)\right]\right)d\tau, \tag{16}$$

where K_0 is a symmetric positive definite matrix.

If the signals associated with a given hypothesis minimize the cost over all possible choices of unknown signals, then the hypothesis is termed optimal. The value of the associated state trajectory is considered as the optimal (minimum-energy) state estimate at time T.

As it is evident from the cost function, the new measurements arriving at every sample time may yield a different optimal trajectory of the state $R^*(t)$ thus making the problem infinite dimensional. Using Mortensen's approach [14], the optimal filtering problem is broken into a recursive filtering equation and a gain update equation. A second-order minimum energy filter for attitude estimation has been provided in [19]. The optimality gap between the full order minimum energy filter and its second-order approximation is small and an analytical upper-bound on this gap has been provided in [16]. Alternatively, in [19, 20] the upper bound on the optimality gap $W(t)$, has also been calculated using a candidate Lyapunov function, and rearranging the terms after differentiating it along the trajectories of the system. The

Initialization:
$$\hat{R}(t_0) = \hat{R}_0, \, K(t_0) = K_0,$$

Filtering:
$$\dot{\hat{R}} = \begin{cases} \hat{R}(\hat{\omega}(t)_\times - \mathbb{P}_a(KY^T\hat{R})) & \text{with } \omega \text{ measurement,} \\ -\hat{R}\mathbb{P}_a(KY^T\hat{R}) & \text{without } \omega \text{ measurement,} \end{cases}$$

$$\dot{K}(t) = \frac{1}{2}Q - K(Y^T\hat{R} + \hat{R}^TY)K + K(t)\hat{\omega}(t)_\times - \hat{\omega}(t)_\times K(t),$$

$$\mathbb{P}_a(X) = \frac{1}{2}(X - X^T).$$

relationship between the cost J incurred by the second-order approximation of minimum energy filter, the optimal cost J^* of the optimal minimum energy filter, and the upper bound $W(t)$ on the optimality gap, is given by

$$J - J^* = J - \frac{1}{4}\int_0^T trace\left[\left(Y^TR - I\right)^T\left(Y^TR - I\right)\right]d\tau \le W(t). \tag{17}$$

For the system described by (1), the second-order minimum energy filter is given in Table 2, see [19, 20] for details.

C. Attitude Observer on $SO(3)$

The attitude observer on $SO(3)$ consists in the same filtering equation as that of a minimum energy filter, given in Table 2. The gain of the observer, instead of evolving as a solution of the Riccati equation as for the minimum energy filter, is set to a constant matrix which can be found in a number of ways. In the present case it was observed that a favorable trade-off between convergence and steady-state performance can be obtained if the observer gain is set equal to the steady-state gain matrix of the minimum energy filter.

It is noted that although the fixed-gain observer is not an optimal estimator, it is free from the instabilities which may arise from the numerical integration of the Riccati equation in an optimal or near-optimal filter.

D. 2nd Order Minimum Energy Filter

A further development of the presented minimum energy filter on $SO(3)$ was introduced by Saccon *et al* [21]. In the cited paper an explicit formula for a second-order optimal nonlinear filter on general Lie groups was developed. As an example, the Authors develop a second-order filter on $SO(3)$ which depends on the choice of affine connection which encodes the nonlinear geometry of the state space. When the symmetric Cartan-Shouten (0)-connection is chosen, the filter has the familiar form of a gradient estimator along with a perturbed Riccati-type matrix differential equation which

9

describes the evolution of the filter gain.

The second-order minimum energy filter [21] is based on the choice of an affine connection, and it is not straightforward to extend the proposed filter to relative attitude dynamics, except for the special case of non-rotating chaser spacecraft, *i.e.*,

$$\dot{\omega} = RI_t^{-1} \left[-\omega_t|_{\mathcal{T}} \times I_t \omega_t|_{\mathcal{T}} \right] + B\delta. \tag{18}$$

Since the chaser spacecraft cannot always be expected to be non-rotating in real applications, this assumption of a non-rotating chaser spacecraft limits the practical use of this formulation of second-order minimum energy filter for a generic relative attitude estimation problem. To generalize this method to the case of an arbitrarily rotating chaser spacecraft, a different affine connection has to be developed by incorporating the relative attitude dynamics (9) and that will result into a slightly different filtering formulation. However, this is not the goal of this paper. The measurements are assumed to be the noisy line of sight vectors r_i, as:

$$r_i = R^T \bar{r}_i + d_i \epsilon, \tag{19}$$

where ϵ is the measurement noise vector and d_i is the scaling factor.

The complete formulation of the second-order filter on $SO(3)$ for (18) and the symmetric Cartan-Shouten (0)-connection is provided in Table 3.

E. 2nd Order Minimum Energy Filter without Dynamics

As highlighted in Section III.D, the use of an affine connection in estimating the angular velocity limits the applicability of a second-order minimum energy filter for generic relative attitude estimation problems beyond the special case of a non-rotating chaser spacecraft. Furthermore, for the cases of uncooperative objects in space (*e.g.*, derelict satellites, space debris), the inertia matrix of the target is usually uncertain. Therefore, a slightly different formulation of the second-order minimum energy filter is proposed in the following. In fact, a simplification to the filter proposed in [21] is introduced without considering the dynamics of the system. In particular:

$$\dot{R} = R \left(\omega(t) \right)_{\times}, \tag{20}$$

$$\dot{\omega} = B\delta. \tag{21}$$

Equations (20) and (21) are directly expressed in relative terms and in the chaser frame, not relying on the dynamics equation. It is worth underlying that this formulation does not require the knowledge of the inertia matrix. This is very important when the inertia matrix of the body is uncertain or completely unknown, as in the case of derelict satellites or asteroids.

10

Table 3   The 2nd order minimum energy filter on $SO(3)$

Initialization:	
	$$\hat{R}(t_0) = \hat{R}_0, \ \hat{\omega}(t_0) = \hat{\omega}_0, \ K(t_0) = K_0,$$

Filtering:

$$\dot{\hat{R}} = \hat{R} \left(\hat{\omega}(t) + K_{11}\boldsymbol{r}^R + K_{12}\boldsymbol{r}^\omega \right)_\times,$$

$$\dot{\hat{\omega}} = I_t^{-1} \left((I_t\hat{\omega})_\times \hat{\omega} + \boldsymbol{\tau} \right) + K_{21}\boldsymbol{r}^R + K_{22}\boldsymbol{r}^\omega,$$

$$\dot{K}(t) = -\alpha K + AK + KA^T - KEK + BR^{-1}B^T - WK - KW^T,$$

where

$$\begin{bmatrix} \boldsymbol{r}^R \\ \boldsymbol{r}^\omega \end{bmatrix} = \begin{bmatrix} -u_1(\hat{\boldsymbol{r}}_1 \times \boldsymbol{r}_1) - u_2(\hat{\boldsymbol{r}}_2 \times \boldsymbol{r}_2) \\ \boldsymbol{0} \end{bmatrix},$$

$$u_i = \frac{b^2}{d_i^2},$$

$$\hat{\boldsymbol{r}}_i = \hat{R}^T \bar{\boldsymbol{r}}_i, \quad \boldsymbol{r}_i = \hat{R}^T \bar{\boldsymbol{r}}_i + d_i\boldsymbol{\epsilon},$$

$$A = \begin{bmatrix} -\hat{\omega}_\times & I \\ 0 & RI_t^{-1} \left[(I_t\hat{\omega}) - \hat{\omega}_\times I_t \right] \end{bmatrix},$$

$$E = \begin{bmatrix} \sum_{i=1}^{2} \boldsymbol{u}_i \left((\hat{\boldsymbol{r}}_i)_\times (\boldsymbol{r}_i)_\times + (\boldsymbol{r}_i)_\times (\hat{\boldsymbol{r}}_i)_\times \right)/2 & 0 \\ 0 & 0 \end{bmatrix},$$

$$BR^{-1}B^T = \begin{bmatrix} 0 & 0 \\ 0 & BR^{-1}B^T \end{bmatrix}$$

$$W = \begin{bmatrix} \frac{1}{2} \left(K_{11}\boldsymbol{r}^R + +K_{12}\boldsymbol{r}^\omega \right)_\times & 0 \\ 0 & 0 \end{bmatrix}.$$

Table 4 The 2nd order minimum energy filter on $SO(3)$ (without dynamics)

Initialization:

$$\hat{R}(t_0) = \hat{R}_0, \, \hat{\omega}(t_0) = \hat{\omega}_0, \, K(t_0) = K_0,$$

Filtering:

$$\dot{\hat{R}} = \hat{R} \left(\hat{\omega}(t) + K_{11} \boldsymbol{r}^R + K_{12} \boldsymbol{r}^\omega \right)_\times,$$

$$\dot{\hat{\omega}} = K_{21} \boldsymbol{r}^R + K_{22} \boldsymbol{r}^\omega,$$

$$\dot{K}(t) = -\alpha K + AK + KA^T - KEK + BR^{-1}B^T - WK - KW^T,$$

where

$$\boldsymbol{r}_t = \begin{bmatrix} \boldsymbol{r}^R \\ \boldsymbol{r}^\omega \end{bmatrix} = \begin{bmatrix} -\boldsymbol{u}_1(\hat{\boldsymbol{r}}_1 \times \boldsymbol{r}_1) - \boldsymbol{u}_2(\hat{\boldsymbol{r}}_2 \times \boldsymbol{r}_2) \\ \boldsymbol{0} \end{bmatrix},$$

$$u_i = \frac{b^2}{d_i^2},$$

$$\hat{\boldsymbol{r}}_i = \hat{R}^T \bar{\boldsymbol{r}}_i, \quad \boldsymbol{r}_i = \hat{R}^T \bar{\boldsymbol{r}}_i + d_i \boldsymbol{\epsilon},$$

$$A = \begin{bmatrix} -\hat{\omega}_\times & I \\ 0 & 0 \end{bmatrix},$$

$$E = \begin{bmatrix} \sum\limits_{i=1}^{2} \boldsymbol{u}_i \left((\hat{\boldsymbol{r}}_i)_\times (\boldsymbol{r}_i)_\times + (\boldsymbol{r}_i)_\times (\hat{\boldsymbol{r}}_i)_\times \right)/2 & 0 \\ 0 & 0 \end{bmatrix},$$

$$BR^{-1}B^T = \begin{bmatrix} 0_{3\times3} & 0 \\ 0 & BR^{-1}B^T \end{bmatrix}$$

$$W = \begin{bmatrix} \frac{1}{2} \left(K_{11} \boldsymbol{r}^R + + K_{12} \boldsymbol{r}^\omega \right)_\times & 0 \\ 0 & 0 \end{bmatrix}.$$

The formulation of the kinematic second-order filter (*i.e.*, without the dynamics terms) is summarized in Table 3.

IV. Simulation Scenarios

Since the objective of this study is to compare the performance of the filtering algorithms described above for relative attitude estimation of uncooperative space objects, a torque-free tumbling motion has been simulated for the target spacecraft. In particular, the relative rotational motion has been simulated according to (9). In our simulation cases, we assumed, for simplicity, that the chaser spacecraft is not rotating and therefore $\omega_c = [0 \ 0 \ 0]^T$, for which (9) reduces to (18). The angular velocity of the target depends on the simulation case and it is reported in Table 5.

The motion has been simulated using the Euler equation for rigid body, using the inertia matrix of the Envisat spacecraft [22] as

$$I = \begin{bmatrix} 16979.74 & 0 & 0 \\ 0 & 124801.21 & 0 \\ 0 & 0 & 129180.25 \end{bmatrix} kgm^2. \tag{22}$$

The measurements are generated at 10 Hz transforming the relative rotation matrix to Euler angles and adding noise to each of the three angles according to a normal distribution with zero mean and a standard deviation of 1×10^{-3} rad. This noise level is representative of commonly used vision-based attitude determination techniques [7]. Moreover, for a more complete comparison, the MEKF and the minimum energy filter are also tested for the hypothetical case when angular velocity measurements of the target body are also available. The process noise for this hypothetical case, which reflects the mismatch between measured and actual angular velocity, was modeled according to a normal distribution with zero mean and a standard deviation of 6×10^{-2} rad/s. It is worth emphasizing that this measurement is not available when dealing with uncooperative objects unless the target body is cooperative and its gyro measurements are accessible from the chaser spacecraft. Since all the filters being considered assume different process and measurement models, all of these filters are individually tuned for a good tradeoff between convergence and steady-state performance. The MEKF, with and without angular velocity measurement, is tuned with $Q = (1 \times 10^{-3})^2 I_3$, $R = (1 \times 10^{-3})^2 I_3$ and $Q = (6 \times 10^{-2})^2 I_3$, $R = (1 \times 10^{-3})^2 I_3$, respectively. The minimum energy filter with angular velocity measurement is tuned with $Q = (1 \times 10^{-3}/6 \times 10^{-2})^2 I_3$, while for the case without angular velocity measurement we set $Q = 3I_3$. The observer gain is fixed equal to the steady-state values of the gain of the minimum energy filter, *i.e.*, $K_{observer} \equiv 2.1 I_3$. Finally, we take $BR^{-1}B^T = 5 \times 10^{-2} I_3$, $u_i = 6 \times 10^{-2}$ and $\alpha = 1 \times 10^{-3}$ for the second-order minimum energy filter, while $BR^{-1}B^T = 1 \times 10^{-2} I_3$ is used for the second-order minimum energy filter without the dynamics. It is to be reminded that these tuning settings are not claimed to be the best possible settings, rather these settings were found to offer reasonable trade-off between convergence/stability and the steady-state performance. By testing and comparing the filters in various off-design conditions, we make an attempt to decouple the effects of tuning parameters on the

Table 5 Specifications of the cases considered for the simulation study.

Cases	Number of Monte Carlo Runs	Initial Estimation Error (deg)	Measurement Noise Std. (deg)	Object's Angular Velocity (deg/s)	Moment of Inertia
A1	100	$\phi, \theta, \psi \in [-28.6, +28.6]$	$\sigma = 3.4$	$\begin{bmatrix} 1 \\ 0.1 \\ 0.3 \end{bmatrix}$	I
A2	100	$\phi, \theta, \psi \in [-28.6, +28.6]$	$\sigma = 3.4$	$\begin{bmatrix} 5 \\ 0.1 \\ 0.3 \end{bmatrix}$	I
B1	100	$\begin{bmatrix} 10 \\ -10 \\ 10 \end{bmatrix}$	$\sigma \sim WN(3.4, 0.3 \times 3.4)$	$\begin{bmatrix} 1 \\ 0.1 \\ 0.3 \end{bmatrix}$	I
B2	100	$\begin{bmatrix} 10 \\ -10 \\ 10 \end{bmatrix}$	$\sigma \sim WN(3.4, 0.3 \times 3.4)$	$\begin{bmatrix} 5 \\ 0.1 \\ 0.3 \end{bmatrix}$	I
C1	100	$\phi, \theta, \psi \in [-28.6, +28.6]$	$\sigma \sim WN(3.4, 0.3 \times 3.4)$	$\begin{bmatrix} 1 \\ 0.1 \\ 0.3 \end{bmatrix}$	I
C2	100	$\phi, \theta, \psi \in [-28.6, +28.6]$	$\sigma \sim WN(3.4, 0.3 \times 3.4)$	$\begin{bmatrix} 5 \\ 0.1 \\ 0.3 \end{bmatrix}$	I
D	100	$\phi, \theta, \psi \in [-28.6, +28.6]$	$\sigma \sim WN(3.4, 0.3 \times 3.4)$	$\begin{bmatrix} 5 \\ 0.1 \\ 0.3 \end{bmatrix}$	$I \in [I - 0.45I, I + 0.45I]$

performance of the filters.

We are interested in studying the estimation errors, especially their sensitivity to the variations in measurement noise intensity, initial conditions, and angular velocities of the non-cooperative object in space. Therefore, we consider the cases outlined in Table 5, which are used for trajectory generation. The filters, however, are not "*aware*" of the configurations of any test case and are used with the nominal tuning. To cope with initial estimation errors all the first order filters are initialized with

$$K_0 = 5I_3,$$

while the second-order filters are initialized with

$$K_0 = \begin{bmatrix} 42.5I_3 & 0_{3\times3} \\ 0_{3\times3} & 0.909I_3 \end{bmatrix}.$$

All the filters in this study are run with an update rate of 10 Hz.

The cases A1 and A2 are designed to investigate the effect of variations in initial estimation error and in angular velocity of the uncooperative space object. For A1 and A2, the measurements of the true trajectory were simulated with a constant zero-mean measurement noise of standard deviation 6×10^{-2} rad (or 3.4 deg), and the initial attitude was

constructed from a set of Euler angles each of which were uniformly drawn from $\begin{bmatrix} -0.5, +0.5 \end{bmatrix}$ rad (or $\begin{bmatrix} -28.6, +28.6 \end{bmatrix}$ deg). A1 and A2 were simulated with the nominal angular velocity ω_1 (*i.e.*, equal to that of Envisat) and ω_2, respectively, given by:

$$\omega_1 = \begin{bmatrix} 1 \\ 0.1 \\ 0.3 \end{bmatrix} deg/s, \quad \omega_2 = \begin{bmatrix} 5 \\ 0.1 \\ 0.3 \end{bmatrix} deg/s. \tag{23}$$

Both A1 and A2 are run 100 times, using fixed inertia matrix which equals that of Envisat (22).

For cases B1 and B2, the initial conditions are fixed to $\begin{bmatrix} 10 & -10 & 10 \end{bmatrix}^T$ *deg*, and the initial angular velocity is ω_1 and ω_2, respectively. The standard deviation of actual measurement noise which is used in the measurement generation is set to be a random variable. The random variable has a mean equal to the nominal standard deviation σ, and a standard deviation 30% of the nominal standard deviation. Both cases are run 100 times each, but the filters are unaware of the actual measurement noise and therefore are still tuned for the nominal standard deviation. The inertia matrix is kept fixed to the value given in (22) in these simulations and is assumed to be perfectly known.

The cases C1 and C2 are run for 100 times each, and combine the uncertain initial conditions from cases A1 and A2, with the uncertain measurement noise properties from B1 and B2. The inertia matrix is still assumed to be fixed (*i.e.*, Envisat inertia matrix in these cases) and perfectly known a priori.

Finally the case D is run for 100 times, with all the same parameters as that of C2 but with the uncertain inertia matrix this time. The diagonal terms of the inertia matrix are now assumed to be uniformly drawn from a set of $[-45, +45]\%$ of their nominal values. This has been done to evaluate how an inaccurate knowledge of the inertia properties of the body affects the estimation.

A. Single Run (Case C2)

To visualize the convergence and steady-state performance of various filters, results from a single run (under simulation parameters of case C2) are reported in Figure 1 and Figure 2. The metric adopted for the estimation error is the axis-angle representation which yields a scalar measure of distance between two reference frames.

Figure 1 depicts the convergence properties of estimation errors of all the filters under a single run, and therefore only initial 40 seconds are shown. Both variants of MEKF (*i.e.*, with and without angular velocity measurement) are the quickest to converge. This stems from the fact that measurement update step in the MEKF (Table 1, see also [2, 18]) is based on first order approximation of quaternion update and therefore the measurement step is *linear*. The minimum energy filter is slower to converge than the MEKF, due to a fully nonlinear *geometric* measurement update. The minimum energy filter and the $SO(3)$ observer are still quicker to converge as compared to the second-order minimum energy filters, while the minimum energy filter with angular velocity measurement is the slowest to converge.
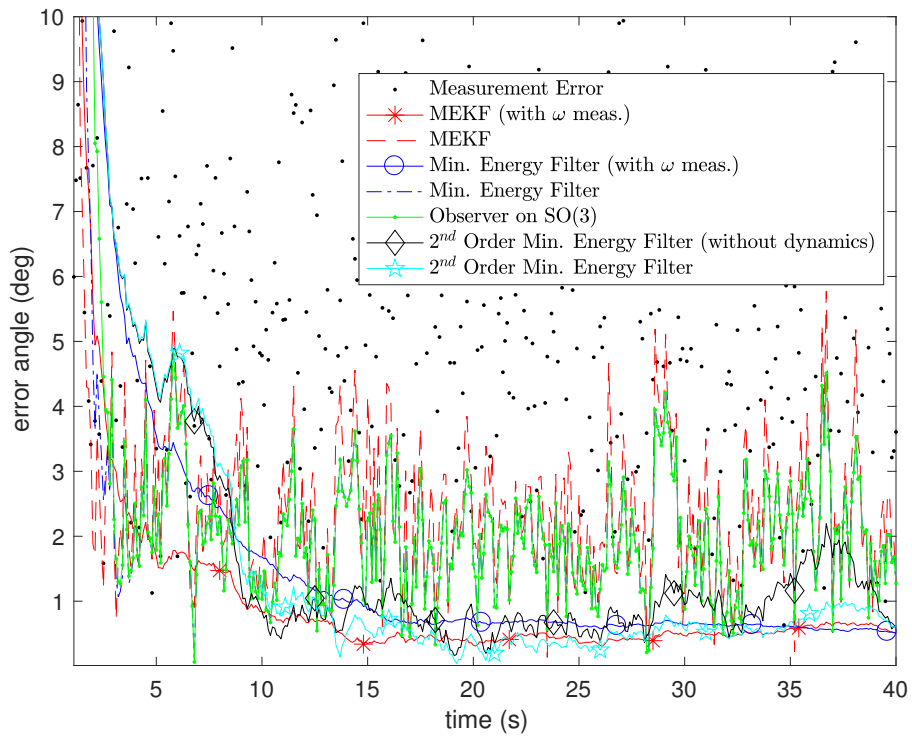
Fig. 1 Estimation errors in a single run (y-axis is in log scale to demonstrate the speed of convergence of different filters).
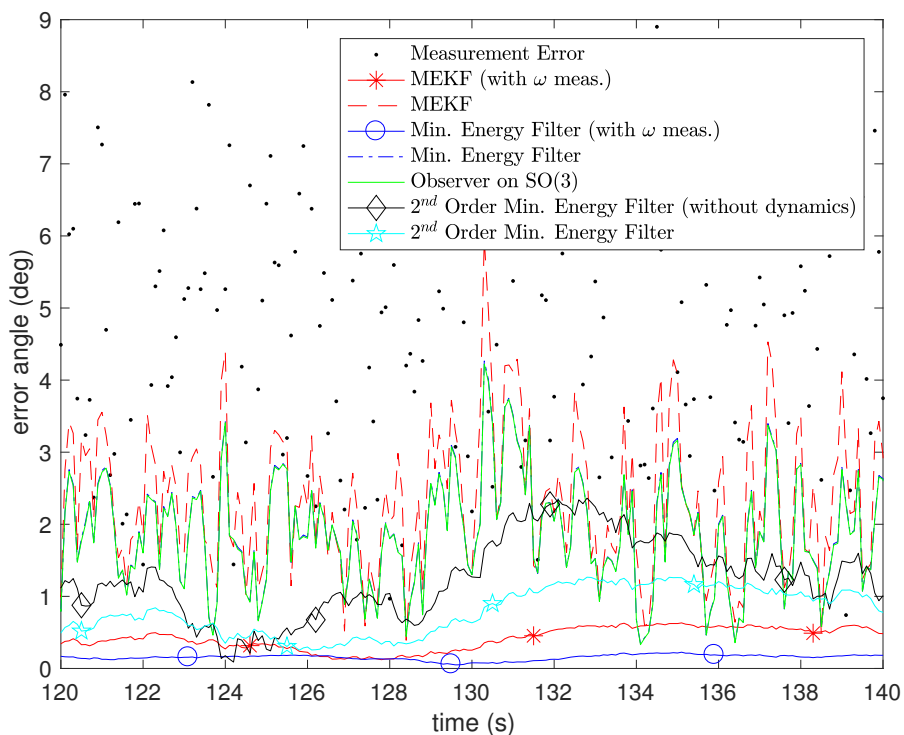
Fig. 2 Estimation errors in a single run (steady-state performance of different filters).

The second-order filters are prone to convergence problems if initialized with a large estimation error, which stems from the fact that second-order filters estimate not only the attitude but also the angular velocity. If initialized with large estimation error, during the convergence the second-order filters *build up* an angular velocity in the direction of convergence and this creates undesired oscillations after the filter has reached steady-state. To circumvent this problem, the angular velocity of second-order filters is not updated for initial 5.5 seconds, and hence the angular velocity is only estimated after 5.5 seconds when the initial transients have vanished. This transient time of 5.5 was chosen because it provided a reasonable trade-off between speed of convergence and the steady-state error.

The slow convergence of the minimum energy filter in comparison to MEKF is in contradiction to [17], but the possible explanation could be that the MEKF adopted in [17] is not the usual MEKF we have considered in this paper, see *e.g.*, [2, 18]. The MEKF used in [17] contains the same nonlinear measurement update equation as the minimum energy filter, and differs from the minimum energy filter only in its gain update equation.

The steady-state performance of the filters, in a single run, is shown in Figure 2. The MEKF turns out to be the worst performer at steady-state, which only slightly improves the measurements. Since the minimum energy filter and the observer designed on $SO(3)$ are equivalent at steady-state, we see that their estimation errors are identical at steady-state. The second-order minimum energy filter (without dynamics) performs better than the minimum energy filter but worse

17
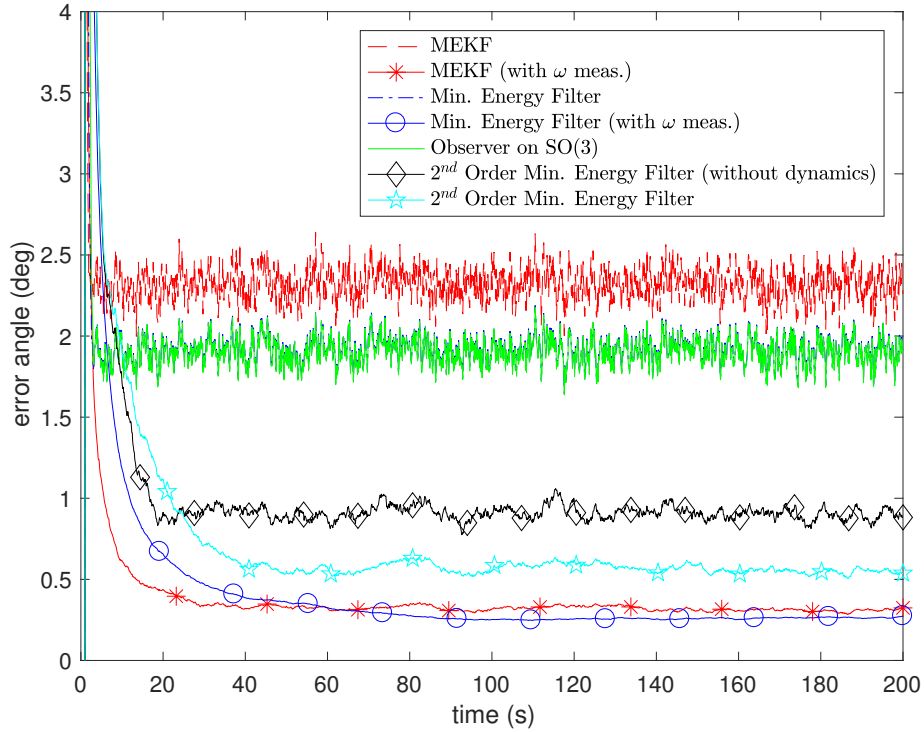
Fig. 3   Estimation errors, averaged over 100 Monte-Carlo runs for simulation case Case A1.

than the second-order minimum energy filter, whose performance nears the performance of the MEKF (with angular measurement) and the minimum energy filter (with angular measurement).

B. Cases A1, A2 [Random Initial Conditions, Known Measurement Noise]

As outlined in Table 5, the cases A1 and A2 are designed to investigate the effect of variations in initial estimation error and in angular velocity of the uncooperative space object. The estimation errors are averaged over 100 Monte-Carlo runs, and presented in Figure 3 and Figure 4 for case A1 and Case A2, respectively. A more quantitative measure of filters performance in transient (i.e., initial 60 seconds) and steady-state (i.e., 60-200 seconds) is the Root Mean Squared (RMS) estimation error which is reported in Table 6, for both cases.

For the case A1, it is evident from Figure 3 and Table 6 that both variants of MEKF are quickest to converge, in comparison with all other filters. The observer on $SO(3)$ and the minimum energy filter also exhibit good convergence properties, while the second-order minimum energy filters are slower than the minimum Energy filter. The minimum Energy filter with angular velocity measurements is the slowest to reach its steady-state error. At the steady-state, the second-order minimum energy filter exhibits the best performance, after the filters which utilize the angular velocity measurements. The second-order minimum energy filter without the dynamics terms containing inertia matrix is slightly worse than the the second-order minimum energy filter, but it is free from the need of accurate absolute attitude estimates

18
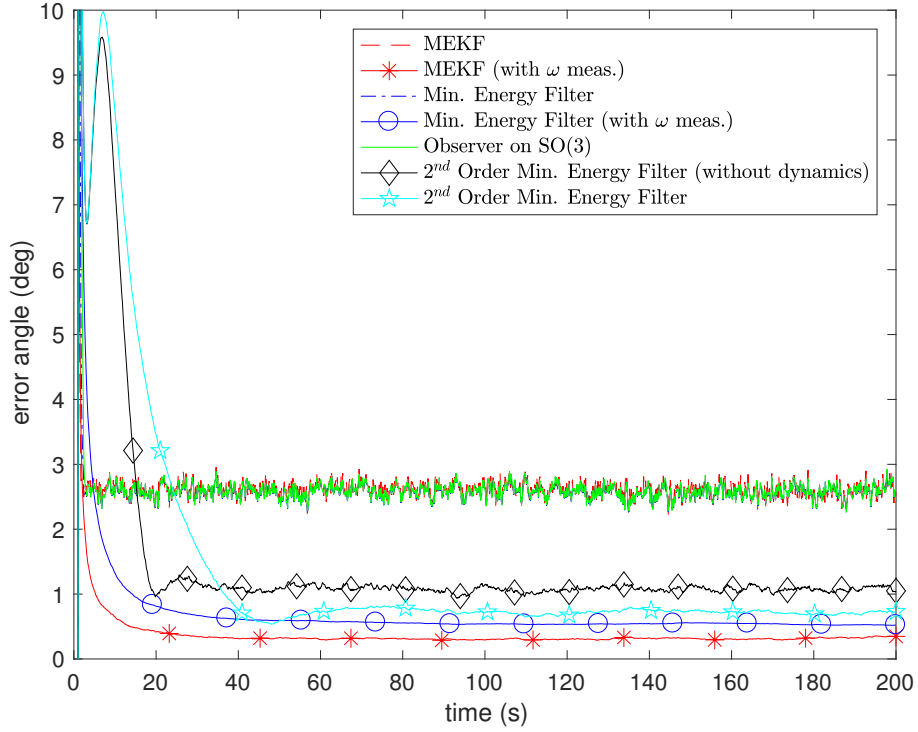
Fig. 4   Estimation errors, averaged over 100 Monte-Carlo runs for simulation case Case A2.

Table 6   Root mean squared values of estimation errors (deg), averaged over 100 Monte-Carlo runs : Cases A1 and A2.

Filters	Transient Error		Steady-State Error	
	Case A1	Case A2	Case A1	Case A2
MEKF (with ω measurement)	1.29	1.19	0.34	0.33
Minimum energy filter (with ω measurement)	2.59	2.57	0.28	0.56
MEKF	2.71	2.97	2.52	2.83
Minimum energy filter	2.88	3.35	2.08	2.76
Observer on $SO(3)$	3.90	4.19	2.06	2.77
2nd order Minimum energy filter	3.37	4.63	0.99	1.15
2nd order Minimum energy filter (with dynamics)	3.35	5.09	0.61	0.78

19

Table 7   Root mean squared values of estimation errors (deg), averaged over 100 Monte-Carlo runs: Cases B1 and B2.

| Filters	Transient Error		Steady-State Error	
	Case B1	Case B2	Case B1	Case B2
MEKF (with ω measurement)	0.70	0.72	0.33	0.33
Minimum energy filter (with ω measurement)	1.63	1.75	0.28	0.57
MEKF	2.53	2.83	2.49	2.79
Minimum energy filter	2.35	2.95	2.05	2.73
Observer on $SO(3)$	2.80	3.31	2.04	2.74
2nd order Minimum energy filter	2.23	3.74	0.97	1.14
2nd order Minimum energy filter (with dynamics)	2.21	4.33	0.59	0.78

as well as from the need to have any idea about the moment of inertia matrix of the target. The minimum energy filter is further significantly worse, but is quite better than the MEKF which is the worst at steady-state. The observer on $SO(3)$ also performs better than MEKF and its steady-state performance is almost identical to the minimum energy filter.

For the case A2, we note from Figure 4 and Table 6 that the performance of almost all the filters deteriorates when tracking the attitude of a body rotating at a higher angular velocity. However, the performance of MEKF, with and without the angular velocity measurement, is less affected and we conjecture that this characteristic of the MEKF also owes its existence to the *linear* measurement update step. The convergence properties of all the filters are similar to case A1, except second-order filters which take quite longer to converge in this case. At the steady-state, second-order filters are still the best performers which tend to achieve the estimation errors closer to filters operating on the angular velocity measurement. The minimum energy filter and the observer on $SO(3)$ perform slightly better than the MEKF, but their filter is significantly worse than the second-order filters.

C. Cases B1,B2 [Known Initial Conditions, Uncertain Measurement Noise]

The cases B1 and B2 are mainly selected to probe the sensitivity of filters' performance under random variations in the measurement noise intensity. The standard deviation of actual measurement noise is assumed to be a random variable in this case. This random variable has a mean equal to the nominal standard deviation σ, and a standard deviation equal to 30% of the nominal standard deviation. Both cases are run 100 times each, but the filters are unaware of the actual measurement noise and therefore are used with the nominal tuning.
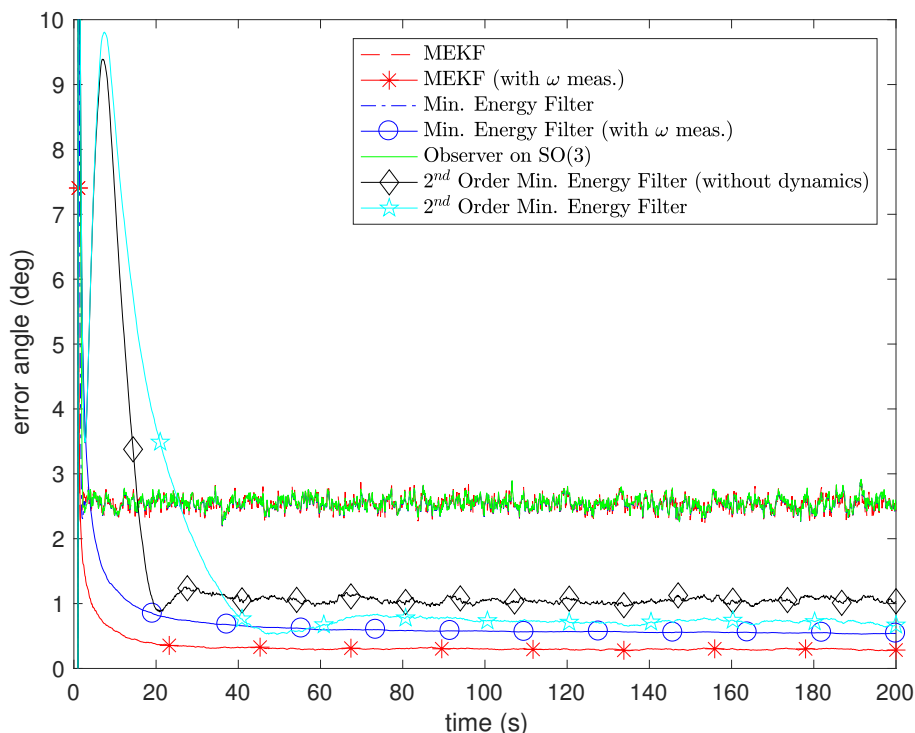
The estimation errors averaged over 100 Monte-Carlo runs are provided in Figure 5 and Figure 6 , for case B1 and
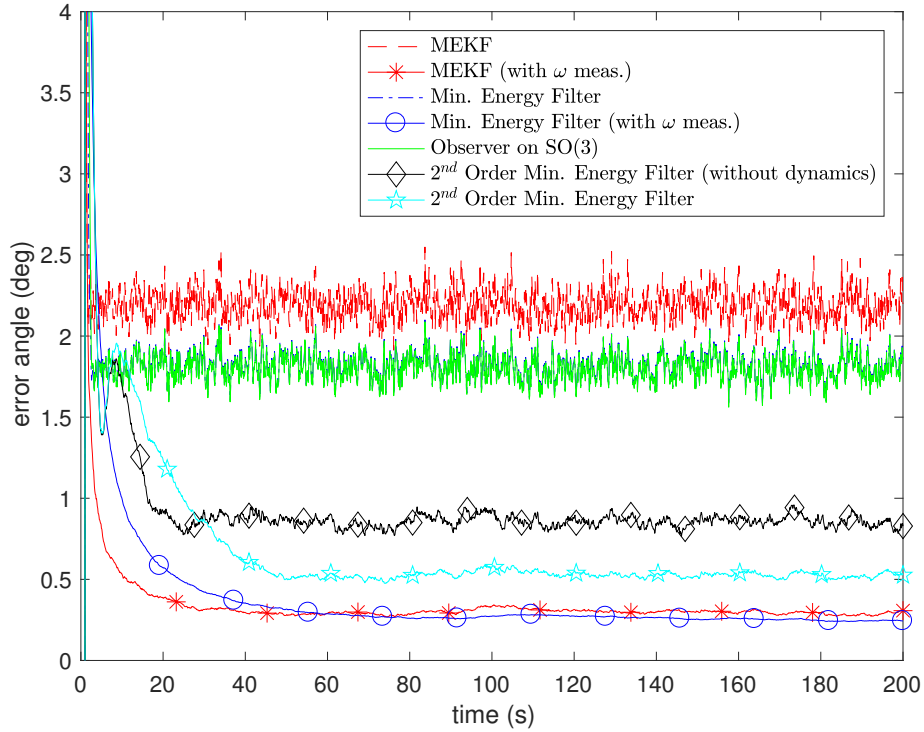
Fig. 5 Estimation errors, averaged over 100 Monte-Carlo runs for simulation case Case B1.

B2, respectively. Table 7 contains the MSE of different filters for a direct comparison. The results are mainly consistent with the results presented in the previous section. The MEKF is the quickest to converge but the worst performer at the steady-state, although with a much lower margin for the case B2. The observer is slower than the minimum energy filter in terms of convergence but, as can be expected, its performance is almost indistinguishable from the minimum energy filter at the steady-state. The minimum energy filter is faster to converge as compared to the second-order minimum energy filters, but at the expense of considerable degradation in performance at the steady-state. The second-order minimum energy filter without dynamics remarkably improves the performance in comparison with the minimum energy filter, and the second-order minimum energy filter slightly improves it further close to the order of filters which utilize angular velocity measurement. The convergence of second-order filters is, however, worse than the minimum energy filter and they are prone to oscillations if initialized with a large estimation error especially for the higher angular velocity case (*i.e.*, case B2).

Furthermore, we also notice the same trends of degradation in steady-state performance in higher angular velocity case, and the performance of the MEKF suffers the least also in this case.

Fig. 6   Estimation errors, averaged over 100 Monte-Carlo runs for simulation case Case B2.

D. Cases C1, C2 [Random Initial Conditions, Uncertain Measurement Noise]

The case C1 and C2 combine the uncertain initial conditions from Case A1 and A2, with the uncertain measurement noise properties from B1 and B2. The inertia matrix is still assumed to be fixed and perfectly known. The estimation errors averaged over 100 Monte-Carlo runs are presented in Figure 7 and Figure 8 , for case C1 and D2, respectively. While the MSE achieved of different filters are illustrated in Table 8.

The MEKF is the fastest to converge, to be followed by the observer on $SO(3)$ and the minimum energy filter. The second-order minimum energy filters are slowest to converge, especially in the higher angular velocity case. The minimum Energy filter with angular velocity measurement is the slowest to converge, due to the fully nonlinear measurement update. The steady-state properties of the observer on $SO(3)$ and the minimum energy filter are much better than the MEKF in the case C1, but only slightly better in the case C2. The second-order minimum energy filter, as in previous test cases, tends to approach the performance of filters utilizing the angular velocity measurement but it requires the knowledge of the inertia matrix as well as the reliable absolute attitude estimates. The steady-state performance of the second-order minimum energy filter without the dynamics term is very close to the performance of the second-order minimum energy filter in both cases, but with the added advantage that it does not require any knowledge about the inertia matrix or the absolute attitude of the chaser spacecraft.
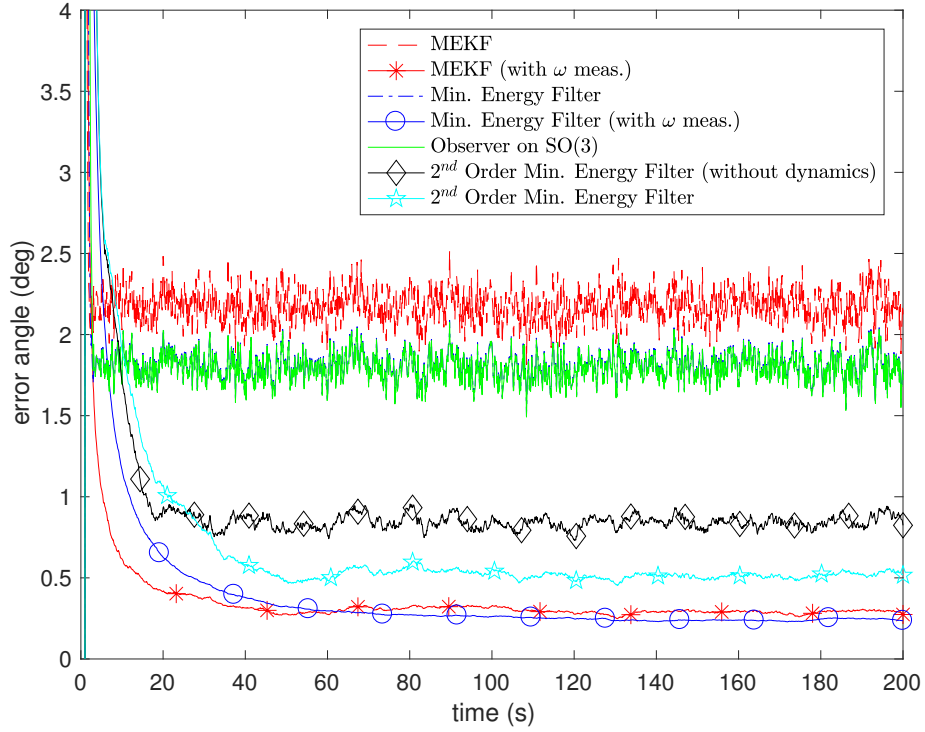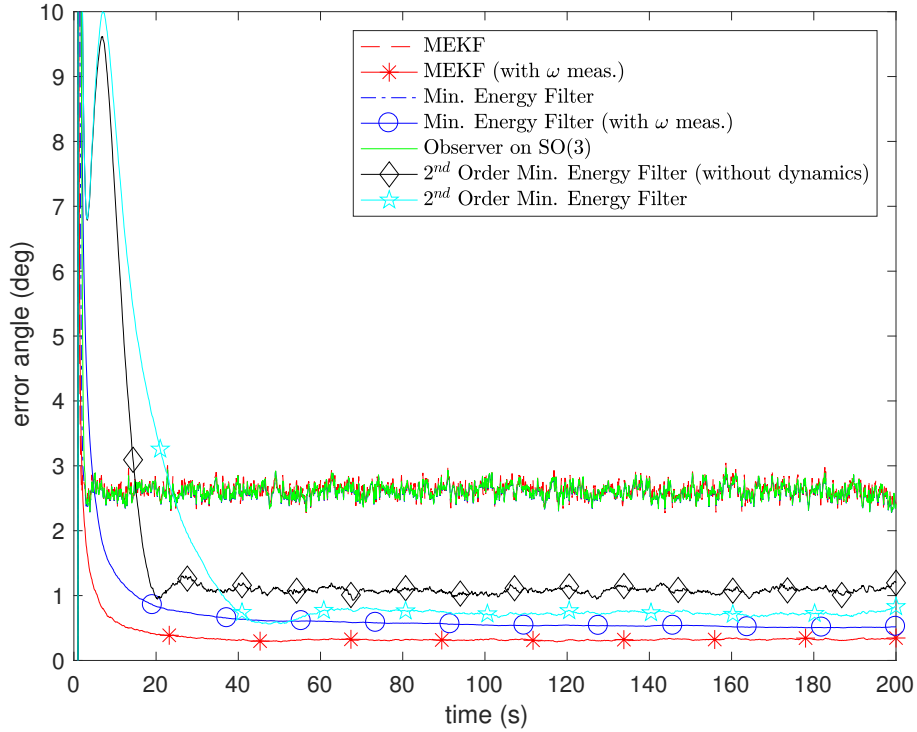
Fig. 7 Estimation errors, averaged over 100 Monte-Carlo runs for simulation case Case C1.

Table 8 Root mean squared values of estimation errors (deg), averaged over 100 Monte-Carlo runs: Cases C1 and C2.

Filters	Transient Error		Steady-State Error	
	Case C1	Case C2	Case C1	Case C2
MEKF (with ω measurement)	1.31	1.21	0.33	0.35
Minimum energy filter (with ω measurement)	2.58	2.64	0.27	0.55
MEKF	2.67	3.03	2.47	2.91
Minimum energy filter	2.86	3.41	2.04	2.82
Observer on $SO(3)$	3.85	4.26	2.03	2.83
2nd order Minimum energy filter	3.37	4.65	0.96	1.18
2nd order Minimum energy filter (with dynamics)	3.36	5.10	0.59	0.80

Fig. 8   Estimation errors, averaged over 100 Monte-Carlo runs for simulation case Case C2.

E. Case D [Random Initial Conditions, Uncertain Measurement Noise, Uncertain Inertia of the Target]

Finally with the parameters of case D, simulations are run for 100 times where we take the same parameters as that of C2 but with the uncertain inertia matrix this time. The diagonal terms of the Inertia matrix are assumed to be uniformly drawn from a set of $[-45, +45]\%$ of their nominal values.

The Figure 9 and Table 9 contain the results of case D. Since it is exactly the same case as C2 except for the uncertain variations in the inertia matrix, the results are similar to the ones presented in the previous subsection, except for the second-order minimum energy filter which depends on the inertia matrix. With this large uncertainty in the inertia matrix, which is not unusual for uncooperative objects in the space, the performance of the second-order minimum energy filter slightly degrades to a level comparable to the performance of the second-order minimum energy filter without dynamics.

The results in this case suggest that the usage of a second-order minimum energy filter without dynamics term may actually yield better performance than the standard second-order minimum energy filter, both during transients and at the steady-state, when the accurate knowledge of inertia matrix of the target object and the absolute attitude estimates of the chaser spacecraft are not available.
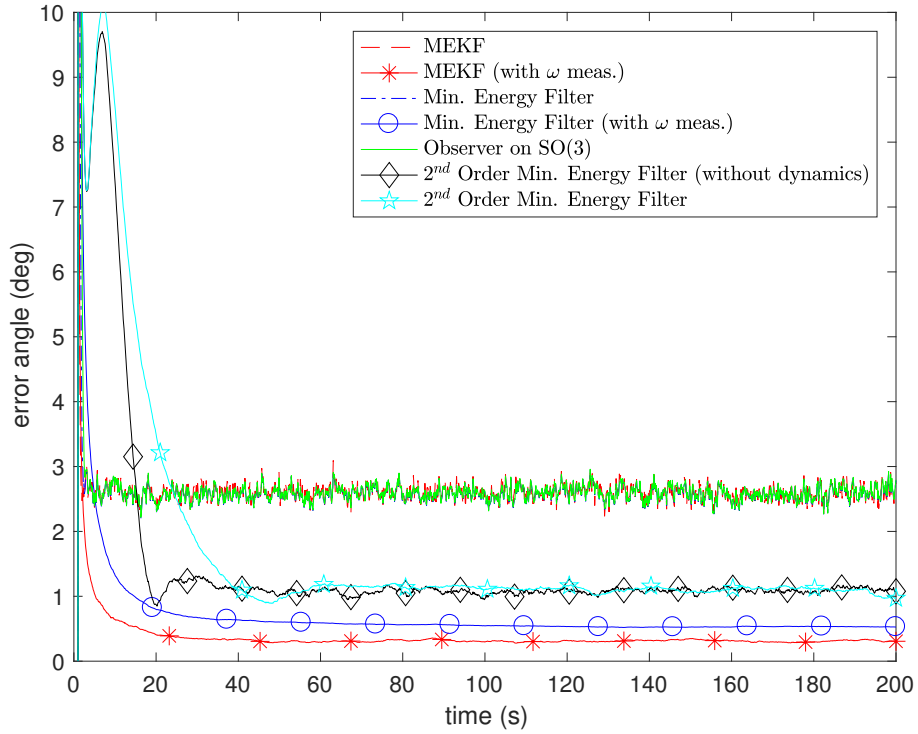
24

Fig. 9   Estimation errors, averaged over 100 Monte-Carlo runs for simulation case Case D.

Table 9   Root mean squared values of estimation errors (deg), averaged over 100 Monte-Carlo runs: Case D.

Filters	Transient Error	Steady-State Error
MEKF (with ω measurement)	1.22	0.35
Minimum energy filter (with ω measurement)	2.60	0.55
MEKF	3.02	2.88
Minimum energy filter	3.39	2.80
Observer on $SO(3)$	4.26	2.81
2nd order Minimum energy filter	4.70	1.18
2nd order Minimum energy filter (with dynamics, uncertain inertia matrix)	5.21	1.28

25

V. Conclusion

The problem of relative attitude estimation for uncooperative objects in space has been considered and potentially promising filtering algorithms have been studied for this specific application. The filtering algorithms have been adapted for this application and compared with the industry standard MEKF. A simulation campaign has been performed evaluating the performance of each filter under different sources of uncertainty. Even if the results change, depending on the simulation case, a general trend can be observed. In fact, it turns out that for this application, although MEKF is the quickest to converge, it loses its edge at the steady-state and has inferior performance to the minimum energy filters or even to an observer at $SO(3)$. The observer on $SO(3)$ has an additional advantage of posing much less computational burden. There is also an added benefit that an observer is not prone to the numerical instabilities which may arise from the numerical integration of Riccati equation. It is to be noted that although the second-order minimum energy filters offer the best performance, the minimum energy filter provides improved performance as compared to MEKF and is significantly simpler in modeling and implementation than the second-order minimum energy filter. For a more demanding application, the second-order minimum energy filter without dynamics has been proposed in this paper and seems to be the best option, since it requires neither an estimate of the absolute attitude nor any knowledge of the inertia matrix. Although the second-order minimum energy filter is the best performer at the steady-state, it may be outperformed by the second-order minimum energy filter without dynamics, when accurate estimates of the target's inertia matrix and absolute attitude of the chaser spacecraft are not available. It should also be pointed out that during the extensive sensitivity analysis of the filter performance with varying update rates, the performance of the minimum energy filter was found to be improving with the increase in update rate of the filter.

References

[1] Markley, F. L., Crassidis, J. L., and Cheng, Y., "Nonlinear attitude filtering methods," *AIAA Guidance, Navigation, and Control Conference*, 2005, pp. 15–18.

[2] Markley, F. L., and Crassidis, J. L., *Fundamentals of spacecraft attitude determination and control*, Vol. 33, Springer, 2014.

[3] Cocaud, C., and Kubota, T., "Autonomous navigation near asteroids based on visual SLAM," *Proceedings of the 23rd International Symposium on Space Flight Dynamics, Pasadena, California*, 2012.

[4] Pesce, V., Lavagna, M., and Bevilacqua, R., "Stereovision-based pose and inertia estimation of unknown and uncooperative space objects," *Advances in Space Research*, Vol. 59, No. 1, 2017, pp. 236–251.

[5] Yol, A., Marchand, E., Chaumette, F., Kanani, K., and Chabot, T., "Vision-based navigation in low earth orbit," *Int. Symp. on Artificial Intelligence, Robotics and Automation in Space, i-SAIRAS'16*, 2016.

[6] Shi, J.-F., Ulrich, S., and Ruel, S., "Spacecraft Pose Estimation using Principal Component Analysis and a Monocular Camera," *AIAA Guidance, Navigation, and Control Conference*, 2017, p. 1034.

[7] D'Amico, S., Benn, M., and Jørgensen, J. L., "Pose estimation of an uncooperative spacecraft from actual space imagery," *International Journal of Space Science and Engineering 5*, Vol. 2, No. 2, 2014, pp. 171–189.

[8] Liu, C., and Hu, W., "Relative pose estimation for cylinder-shaped spacecrafts using single image," *IEEE Transactions on Aerospace and Electronic Systems*, Vol. 50, No. 4, 2014, pp. 3036–3056.

[9] Kanani, K., Petit, A., Marchand, E., Chabot, T., and Gerber, B., "Vision based navigation for debris removal missions," *63rd International Astronautical Congress*, 2012.

[10] Kicman, P., Lisowski, J., Bidaux-Sokolowski, A., and Gil-Fernandez, J., "Advanced vision-based navigation for approach and proximity operations in missions to small bodies," *6th European Conference for Aeronautics and Space Sciences*, 2015.

[11] Segal, S., and Gurfil, P., "Effect of kinematic rotation-translation coupling on relative spacecraft translational dynamics," *Journal of Guidance, Control, and Dynamics*, Vol. 32, No. 3, 2009, pp. 1045–1050.

[12] Crassidis, J. L., Markley, F. L., and Cheng, Y., "Survey of nonlinear attitude estimation methods," *Journal of Guidance, Control, and Dynamics*, Vol. 30, No. 1, 2007, pp. 12–28.

[13] Crassidis, J. L., and Markley, F. L., "Unscented filtering for spacecraft attitude estimation," *Journal of Guidance, Control, and Dynamics*, Vol. 26, No. 4, 2003, pp. 536–542.

[14] Mortensen, R., "Maximum-likelihood recursive nonlinear filtering," *Journal of Optimization Theory and Applications*, Vol. 2, No. 6, 1968, pp. 386–394.

[15] Zamani, M., Trumpf, J., and Mahony, R., "Minimum-energy filtering for attitude estimation," *IEEE Transactions on Automatic Control*, Vol. 58, No. 11, 2013, pp. 2917–2921.

[16] Zamani, M., Trumpf, J., and Mahony, R., "On the distance to optimality of the geometric approximate minimum-energy attitude filter," *American Control Conference (ACC), 2014*, 2014, pp. 4943–4948.

[17] Zamani, M., Trumpf, J., and Mahony, R., "Nonlinear attitude filtering: a comparison study," *arXiv preprint arXiv:1502.03990*, 2015.

[18] Crassidis, J. L., and Junkins, J. L., *Optimal estimation of dynamic systems*, CRC press, 2011.

[19] Zamani, M., Trumpf, J., and Mahony, R., "Near-optimal deterministic filtering on the rotation group," *IEEE Transactions on Automatic Control*, Vol. 56, No. 6, 2011, pp. 1411–1414.

[20] Zamani, M., Trumpf, J., and Mahony, R., "Near-optimal deterministic attitude filtering," *49th IEEE Conference on Decision and Control (CDC), 2010*, IEEE, 2010, pp. 6511–6516.

[21] Saccon, A., Trumpf, J., Mahony, R., and Aguiar, A. P., "Second-order-optimal minimum-energy filters on lie groups," *IEEE Transactions on Automatic Control*, Vol. 61, No. 10, 2016, pp. 2906–2919.

[22] Virgili, B. B., Lemmens, S., and Krag, H., "Investigation on Envisat attitude motion," *e. Deorbit Workshop*, 2014.